NASA Technical Memorandum 4457

Physical Properties of the Benchmark Models Program Supercritical Wing

Bryan E. Dansberry, Michael H. Durham,
Robert M. Bennett, David L. Turnock,
Walter A. Silva, and José A. Rivera, Jr.

SEPTEMBER 1993

NASA Technical Memorandum 4457

Physical Properties of the Benchmark Models Program Supercritical Wing

Bryan E. Dansberry, Michael H. Durham,
and Robert M. Bennett
Langley Research Center
Hampton, Virginia

David L. Turnock
Lockheed Engineering & Sciences Company
Hampton, Virginia

Walter A. Silva and José A. Rivera, Jr.
Langley Research Center
Hampton, Virginia

Abstract

The goal of the Benchmark Models Program is to provide data useful in the development and evaluation of aeroelastic computational fluid dynamics (CFD) codes. To that end, a series of three similar wing models are being flutter tested in the Langley Transonic Dynamics Tunnel. These models are designed to simultaneously acquire model response data and unsteady surface pressure data during wing flutter conditions. The supercritical wing is the second model of this series. It is a rigid semispan model with a rectangular planform and a NASA SC(2)-0414 supercritical airfoil shape. The supercritical wing model was flutter tested on a flexible mount, called the Pitch and Plunge Apparatus, that provides a well-defined, two-degree-of-freedom dynamic system. This report describes the supercritical wing model and associated flutter test apparatus and includes experimentally determined wind-off structural dynamic characteristics of the combined rigid model and flexible mount system.

Introduction

A significant number of aircraft aeroelastic problems such as buffet, control-surface buzz, limit-cycle oscillations, and shock-induced oscillations occur at transonic speeds. Conventional flutter is of greatest concern at transonic Mach numbers as well. Aeroelastic analysis using computational fluid dynamics (CFD) codes holds promise for analysis of all these phenomena (ref. 1). Even for the conventional flutter problem, however, the assessment of CFD codes in the transonic Mach number regime is currently far from complete.

One difficulty in the evaluation of CFD codes is the lack of well-documented experimental data sets. Some of the existing data sets, for example, provide only the flutter boundary defined in terms of the test conditions such as dynamic pressure and Mach number at flutter with the flutter frequency sometimes omitted. Few of the flutter investigations provide quantitative details of the flow field at the flutter condition. These data sets are useful as a guide for CFD code evaluation, but when analytical and experimental results do not correlate well, there is often not enough information available to determine the source of the discrepancy.

Recognizing this difficulty, the Structural Dynamics Division of the Langley Research Center initiated the Benchmark Models Program (BMP). This wind-tunnel test program investigates unsteady flow phenomena to facilitate the development and evaluation of computational aeroelastic codes (refs. 2 to 6). Also, the BMP is assisting in CFD code evaluation by performing tests that produce combined flutter and unsteady pressure data sets. Some flutter tests are conducted on a series of rigid, instrumented semispan models with a flexible mount. This flexible mount system, the Pitch and Plunge Apparatus (PAPA), allows the rigid models to achieve classical flutter by using a well-defined dynamic system. The tests of the flexible PAPA mount and the rigid, instrumented models produce data including both model and mount dynamic response and unsteady surface pressures recorded at flutter.

The supercritical wing described in this report is the second in a series of three similar models that the BMP is testing in the Langley Transonic Dynamics Tunnel (TDT) with the PAPA mount. All three models are rigid rectangular wings with the same planform but with different airfoil shapes. All three models have nearly identical wind-off dynamic characteristics because these characteristics are determined by the flexible PAPA mount. The first model to be tested in this series was the NACA 0012 model. A description of this model and the test results obtained with it are found in references 4 and 5. The third model in this series has an NACA 64A010 airfoil.

This report correlates CFD results with the experimental data acquired with this supercritical wing model. Included in the report are complete descriptions of the model, the PAPA mount, and associated test hardware. Experimentally determined wind-off structural dynamic properties, model airfoil shape, and pressure orifice locations are also included.

Symbols and Abbreviations

A_z	amplitude of plunge motion, in.
A_θ	amplitude of pitch motion, deg
BMP	Benchmark Models Program
CFD	computational fluid dynamics
FFT	fast Fourier transform
f_z	wind-off plunge mode frequency, Hz
f_θ	wind-off pitch mode frequency, Hz
GVT	ground vibration test
PAPA	Pitch and Plunge Apparatus
SGB	strain gage bridge
x	chordwise distance from wing leading edge, in.
x/c	fraction of chord length
y	spanwise distance from wing root, in.
z	vertical distance from wing leading edge, in.
ζ	fraction of critical damping
ζ_z	fraction of critical damping for plunge mode
ζ_θ	fraction of critical damping for pitch mode

Test Apparatus

Model Description

The supercritical wing used in this test has a simple rectangular planform and a NASA SC(2)-0414 second generation supercritical airfoil section. The chord of the model is 16 in. and the span is 32 in. These dimensions result in a panel aspect ratio of 2. At the 32-in-span station, the model terminates in a tip of revolution where the radius is equal to half the airfoil thickness at each position along the chord. Figure 1 presents a top-view sketch of the model.

Figure 2 shows an outline of the NASA SC(2)-0414 supercritical airfoil section. This section was selected from several airfoils described in reference 7. The SC(2) designation indicates it is part of the family of second generation supercritical airfoils, and the 0414 indicates that the airfoil section has a design lift coefficient of 0.4 and a maximum thickness of 14 percent of the chord. The lift coefficient and thickness of the airfoil section were selected because

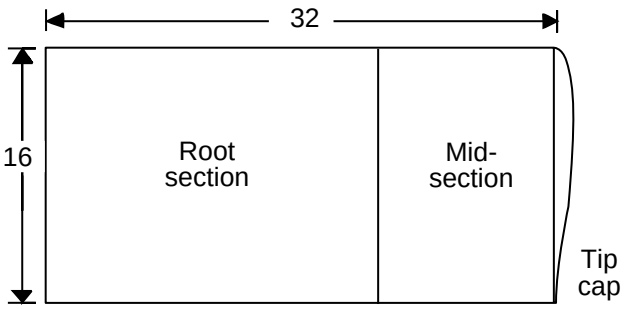

Figure 1. Planform of model. Dimensions are in inches.

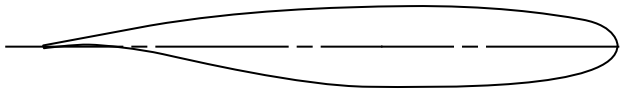

Figure 2. NASA SC(2)-0414 airfoil.

of the flexible PAPA mount load limits and the internal volume required for pressure measurement instrumentation. Prior to flutter testing, the fidelity of the fabricated model with the design airfoil shape was experimentally determined at hundreds of locations on both the upper and lower surfaces. The surface measurements, with only a few exceptions, agreed within a tolerance of ± 0.005 in. with the airfoil design coordinates. The design coordinates and the surface measurement results are in the appendix.

Figure 1 shows the root section, midsection, and tip cap of the supercritical wing. A photograph of the model with the three sections detached is presented in figure 3. The midsection and root

L-91-5715

Figure 3. Model disassembled.

section are solid aluminum with several access holes and the aluminum tip cap is hollow. The inboard and

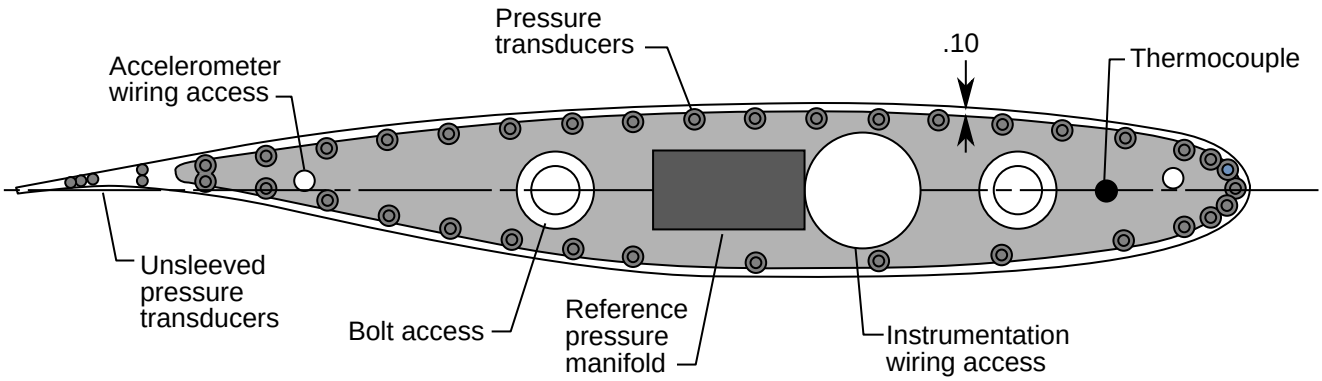

Figure 4. Midsection outboard edge. Dimension is in inches.

outboard edges of these sections are recessed 0.15 in. with a 0.1-in-thick rim. When the root section and midsection are attached, a cavity is created to allow room for instrumentation wiring and reference pressure tubing. Figure 4 is a sketch of the end view of the midsection with the recessed instrumentation cavity shaded.

Figure 4 also shows the access holes for both sections. The large-diameter hole at the 30-percent chord location is a passageway for instrumentation wiring and reference pressure tubing. The 40 small holes near the surface are drilled spanwise 1.25 in. into the sections and are for the installation of the differential pressure transducers. The midsection attaches to the root section with two bolts that are reached through the bolt access holes also shown in the figure.

The break points of the model sections allow access for installation, repair, and removal of the *in situ* pressure measurement instrumentation. To facilitate access to this instrumentation, the midsection and tip cap unbolt from the outboard end so that these sections can be separated and the instrumentation accessed with a minimum of delay and without the removal of the model from the PAPA mount system.

The tip cap is a hollowed out section with a wall thickness of 0.10 in. It is attached to the midsection with two small bolts, each with a shear pin. The seam between the tip cap and midsection is at the 31.8-in-span station, which is 0.2 in. inboard of the tip of revolution. When the tip cap is attached, the two small bolts are recessed below the surface of the tip of revolution and covered with dental plaster to provide a smooth surface.

The supercritical wing contains 80 differential pressure transducers. The 40 housed in the outboard edge of the midsection provide the surface pressure distribution at the 95-percent-span station ($y = 30.4$ in.), and the 40 housed in the outboard edge of the root section provide the surface pressure distribution at the 60-percent-span station ($y = 19.2$ in.). Figure 5 indicates the locations of these two rows of pressure orifices in the spanwise direction. The chordwise distribution of the pressure transducers is identical for both spanwise stations. (See fig. 4.) At each spanwise station there are 23 pressure orifices on the upper surface (including 1 each at the leading and trailing edges) and 17 on the lower surface. The measured x/c locations for all 80 pressure orifices are documented in the appendix.

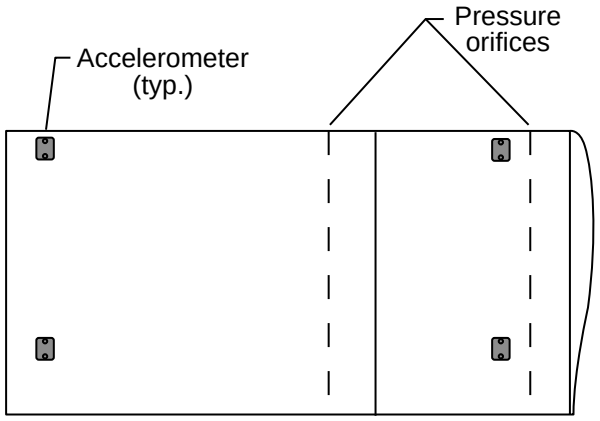

Figure 5. Model instrumentation.

The differential pressure transducers are rated for measurements up to 5 psid and are cylindrical with a nominal diameter of 0.093 in. and a length of 0.6 in. To protect the transducers during installation and removal, most were housed in a protective brass sleeve with an inside diameter of 0.1 in. and an outside

diameter of 0.12 in. However, because the supercritical airfoil is very thin near the trailing edge, modifications in the standard pressure transducer housing arrangement were required and the five pressure transducers located in the most aft positions were installed without brass sleeves (fig. 4). The sleeved and unsleeved transducers were bonded into 0.125-in-diameter holes drilled spanwise 1.25 in. into the outboard end of the model root section and midsection. Figure 6 shows a sketch of an installed transducer and sleeve, while figures 7 to 9 show photographs taken at stages of the installation process.

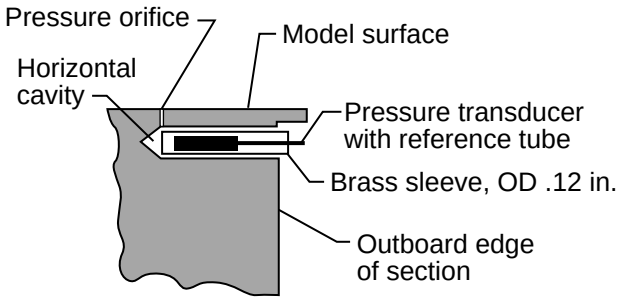

Figure 6. Transducer housing arrangement.

L-91-5716

Figure 7. Midsection before instrumentation.

The surface orifices, 0.018-in. in diameter, were drilled normal to the model surface and connected to the spanwise cavities. Total distance from the surface orifice to the pressure transducer varies between 0.1 and 0.2 in. with only one exception for each chordwise row of measurements. The trailing-edge pressure orifice required a metal tube to be run from the trailing edge forward to an area thick enough to house a pressure transducer. The transmission distance from the trailing-edge orifice to the pressure transducer was approximately 0.7 in.

L-91-07527

Figure 8. Midsection with pressure transducers.

L-91-07526

Figure 9. Pressure transducer reference tubes and manifold in midsection.

Each differential pressure transducer was referenced to free-stream static pressure. At each span station, reference pressure tubes from the 40 transducers were connected to a central manifold (fig. 9). One tube connected this manifold to an area of zero flow in the plenum of the wind tunnel. Free-stream static pressure was constant during each data acquisition period. Since phase matching is unnecessary for a constant pressure, reference pressure transmission distance was not made identical for each transducer. The reference pressure transmission distance was approximately 30 ft.

Four low-frequency accelerometers were housed in the supercritical wing. These accelerometers were used to verify flutter frequency and rigid-body motion during testing. Figure 5 shows the locations of

the four accelerometers on the model. Also, two type T copper-constantan thermocouples were installed, one on the outboard edge of the root section and one on the outboard edge of the midsection. These thermocouples were positioned ahead of the most forward bolt access hole and on the centerline of the airfoil section (fig. 4). They provided a temperature history at one point along each row of pressure transducers for the evaluation of temperature effects on the pressure transducers.

Pitch and Plunge Apparatus Mount

The flexible mount system called the Pitch and Plunge Apparatus (PAPA) provides a well-defined, two-degree-of-freedom dynamic system on which rigid, instrumented models encounter classical flutter in the Transonic Dynamics Tunnel (TDT). (See refs. 8 and 9.) A photograph of the PAPA mount with the splitter plate removed is presented in figure 10.

L-91-321

Figure 10. PAPA mount.

A top-view sketch of the PAPA mount is presented in figure 11. The PAPA mount consists of a moving plate supported from the tunnel wall by a system of four circular rods and a centerline flat-plate drag strut; all connections have fixed-fixed end conditions. The moving plate is made of steel with a thickness of 1 in. and is considered to be rigid. The rods and flat-plate drag strut provide elastic constraints so that the moving plate and attached model will oscillate in pitch and plunge when excited.

At the tunnel wall, the rods and the drag strut are attached to a remotely controlled turntable so that the angle of attack of the model can be varied. The model and PAPA system is limited to 5° of rotation in either the positive or negative direction. The model, however, can attain angles of attack slightly greater than 5° because of twisting of the PAPA mount.

The wind-off characteristics of the rigid-body pitch and plunge modes are largely determined by the length and cross section of the four circular rods and the mass of the moving plate and model. The main purpose of the drag strut is to increase stiffness in the fore and aft (chordwise) direction, thereby separating the natural frequency of the first in-plane mode from that of the plunge mode. Ballast weights can be added to the fore and aft inboard surface of the moving plate. These weights are used to decouple the pitch and plunge modes by moving the center of gravity of the model and PAPA system forward or aft as necessary to locate it on the system elastic axis. The system elastic axis is located at the center of the moving plate and the rod assembly and also corresponds to the midchord of the model. The ballast weights also allow tuning of the total system mass and inertia so that different models can be tested with the same natural frequencies to provide a more meaningful correlation of results between models.

In the wind-tunnel test section, the PAPA mount is located behind a large splitter plate described in the next section. The model attaches to the PAPA moving plate by a short pedestal block that protrudes through an opening in the splitter plate. All loads are transferred from the model to the PAPA mount through this pedestal. The pedestal, which is much shorter than the model in the chordwise direction, sits in a small hole in the splitter plate which is large enough to allow the model and PAPA assembly to translate several inches in the vertical direction without contacting the splitter plate.

Flow through the splitter plate is prevented by a thin, circular end plate at the base of the model, which covers the opening in the splitter plate. The circular end plate has a diameter equal to one chord length and mounts between the pedestal and model. The end plate is recessed into the splitter plate so that the end plate outer surface coincides with the surface of the splitter plate to preserve smooth aerodynamic flow. The inner surface of the end plate is less than 0.1 in. from the recessed portion of the splitter plate, but it is not allowed to rub against this surface. Figure 12 shows the model and end plate mounted in front of the splitter plate in the TDT test section.

Instrumentation on the PAPA includes two calibrated strain gage bridges (SGB's). Each bridge has four arms. One bridge has arms located on the upper

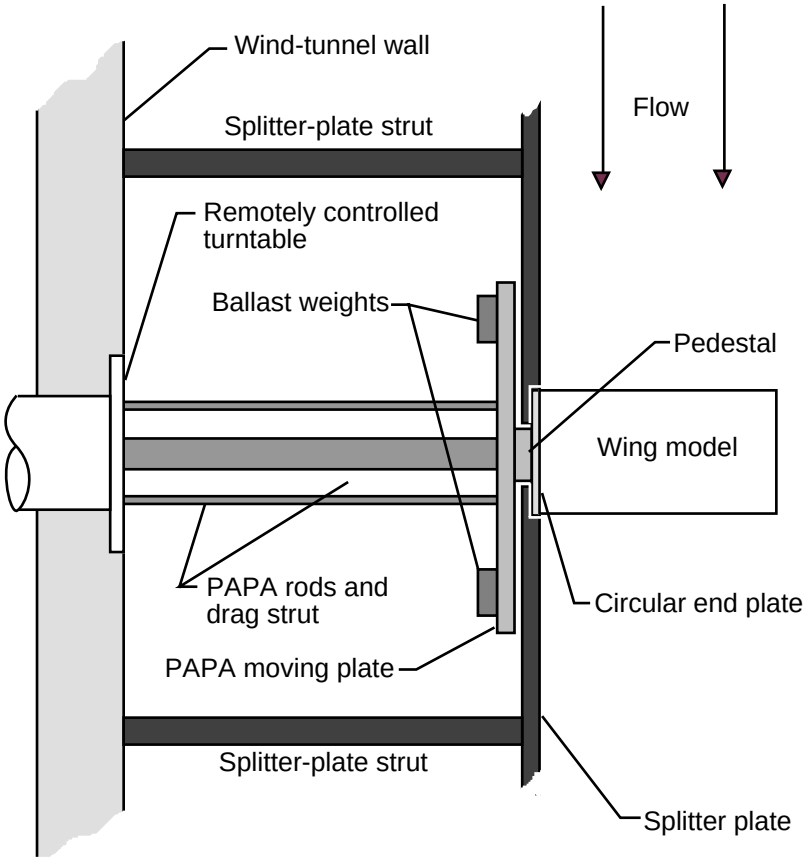

Figure 11. Top view of PAPA mount.

L-91-13738

Figure 12. Model mounted in test section.

and lower surfaces of the drag strut oriented and calibrated to measure vertical loading and vertical displacement. The other bridge has one arm mounted on each of the four circular rods and is oriented and calibrated to measure torsional moment and pitch angle. Two accelerometers are mounted on the inboard side of the moving plate to record pitch and plunge motion. An angle-of-attack accelerometer, which is used to measure the static pitch angle of the moving plate and model, is also located on the inboard surface of the moving plate.

Additional Test Hardware

During wind-on testing, a splitter plate separates the model from the test-section-wall boundary layer and the PAPA hardware. A picture of the model and the splitter plate mounted in the tunnel test section as viewed from upstream is shown in figure 13. The center of the model and PAPA system, and model midchord, is 7 ft from the leading edge of the splitter plate. The splitter plate itself is 12 ft long and 10 ft high and is suspended from the test-section wall by struts that are 40 in. long.

Instrumentation on the splitter plate includes 20 pressure transducers that are the same type used in the model. The transducers are housed in

L-91-16762

Figure 13. Test apparatus.

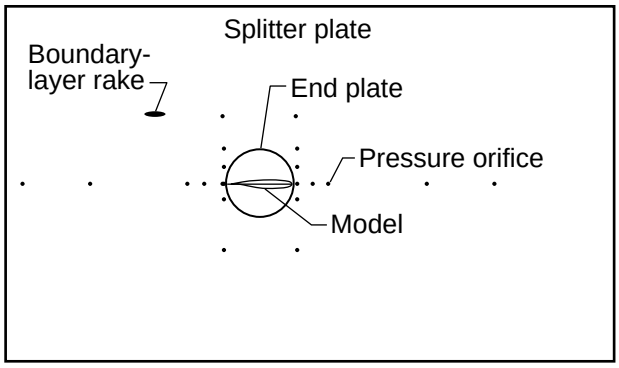

Figure 14. Front view of splitter plate showing instrumentation locations.

brass sleeves and mounted in 0.125-in-diameter holes drilled into the back of the splitter plate, perpendicular to the surface. The orifice holes are 0.018 in. in diameter and connect to the 0.125-in-diameter holes in which the transducers are mounted. The distance from the surface to the pressure transducers is approximately 0.1 in. Locations of the splitter-plate surface pressure orifices are shown in figure 14; coordinates of the locations of the orifices are given in tabular form in the appendix. These measurements provide data on the aerodynamic conditions at the model root plane which could be used to check boundary conditions for CFD analysis.

A boundary-layer rake extends from the splitter-plate surface at a position 16 in. behind and 16 in. above the model trailing edge. This rake houses 10 pressure transducers that measure stagnation pressure to determine the boundary-layer thickness at distances ranging from 0.25 in. to 5 in. from the splitter-plate surface.

The PAPA rods, drag strut, and moving plate are enclosed in an aerodynamic fairing behind the splitter plate. This aerodynamic fairing can be seen in figure 13. The only parts of the apparatus exposed to aerodynamic forces during testing are the supercritical wing and the end plate.

Wind-Off Dynamic Characteristics

A ground vibration test (GVT) of the model and PAPA system was performed to define the natural frequencies and mode shapes prior to flutter testing. In the GVT, frequencies below 190 Hz were investigated. Twelve natural frequencies were identified within this frequency range by rapping the model and performing a fast Fourier transform (FFT) on the measured model response. These natural frequencies are documented in table 1.

Table 1. Natural Frequencies of Model and PAPA System

Mode	Frequency, Hz	Description
1	3.33	Rigid-body plunge (first bending of system)
2	5.20	Rigid-body pitch (first torsion of system)
3	11	First chordwise bending
4	37	First bending of drag strut
5	50	Second bending of system
6	67	Second chordwise bending
7	75	Bending of rod 3
8	78	Bending of rods 1 or 4
9	79	Bending of rods 1 or 4
10	81	Bending of rod 2
11	100	Second bending of drag strut
12	150	Second torsion of system

Figure 15 shows the supercritical wing model and the PAPA moving plate, rods, and drag strut. To determine the mode shapes of the model and PAPA mount, a shaker was used to excite the model at frequencies below 190 Hz. A roving accelerometer, referenced to a load cell mounted at the shaker attachment, was used to measure transfer functions at 44 points on the model and the PAPA mount. The mode shapes corresponding to the natural frequencies below 100 Hz are shown in figure 16. In-plane (chordwise) mode shapes were not investigated, but the natural frequencies of the first two in-plane modes were determined and are included in the data presented in table 1.

Rigid-body plunge and rigid-body pitch are the modes involved in the flutter mechanism. Table 2 summarizes the principal characteristics of these two

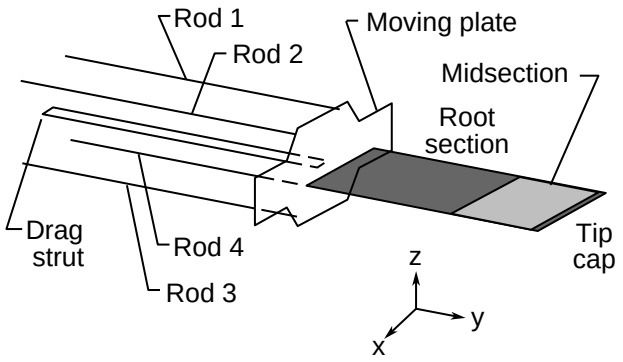

Figure 15. Representation of model and PAPA system.

modes. Frequency, stiffness, and damping values were determined experimentally. Generalized mass values were derived from the measured stiffnesses and frequencies.

Table 2. Properties of Rigid-Body Modes

	Plunge mode	Pitch mode
Frequency	3.33 Hz	5.20 Hz
Stiffness	2637 lb/ft	2964 ft-lb/rad
ζ	0.001	0.001
Generalized mass . . .	6.1 slug-ft^2	2.7 slug-ft^2

The stiffness values for these two modes were determined with static calibrations of the bending and torsion SGB's located on the drag strut and rods of the PAPA. In these calibrations, four weight pans were configured so that loads could be applied, both positive and negative, to the forward and aft portions of the PAPA moving plate. Pure plunge loadings were generated with an equal load applied to the fore and aft ends of the moving plate, while pitch moments were generated with an unequal load distribution.

Four calibrations of the SGB's were performed and consisted of incremental increases in loading to a maximum value followed by incremental decreases in loading. Raw data from these four SGB calibrations are presented in table 3. In this table, the individual plunge and pitch loadings are given along with the leading- and trailing-edge vertical displacements. Plunge loading is positive as a lifting load, while pitch loading is positive when the leading edge twists up. Vertical displacements z are positive for lifting loads.

Verifications of the natural frequencies and structural damping characteristics of the plunge and pitch modes were periodically performed between wind-on test runs. These results verified that no significant changes in the primary modes occurred as a result of the many flutter points experienced by the model and PAPA system. These verifications consisted of manually exciting the system in the plunge mode and recording data as the model motion decayed; then the process was repeated for the pitch mode. Three sets of 20-sec data records were acquired for each mode: one at high amplitude, one at medium amplitude, and one at low amplitude. Sections of these data records were then analyzed for frequency and damping using a least-squares fitting technique. This allowed the nonlinear effects of amplitude on frequency and damping to be studied within individual data sets.

Results of these frequency and damping checks are reported in tables 4 and 5. In these tables separate data records are denoted by numbers, while sections of the same data set analyzed separately are denoted by letters.

Figures 17 and 18 show the values of the rigid-body plunge and pitch mode frequencies recorded during these checks. In these figures, the horizontal line indicates the frequency for the modes given in table 2. The range of mean amplitudes at flutter for which data were recorded indicates which of these data are of greatest importance. The second-order curve fits are good approximations of the variation in frequency with increasing amplitude for these modes. They show that there is a slight decrease in plunge mode frequency and a slight increase in pitch mode frequency with increasing amplitude. These variations are less than 0.02 Hz across the range of flutter amplitudes at which data were recorded.

Figures 19 and 20 show the damping recorded during the frequency and damping checks. The damping shown in table 2 is represented by the horizontal lines. The range of amplitudes at flutter for which data were recorded is indicated as well. In these figures, linear curve fits give good approximations of the variation in damping with amplitude. These curve fits show that damping increases slightly with increasing amplitude. The variations are small and their significance would depend on the sensitivity of the flutter mechanism to damping.

A series of four points in figure 20, which deviate slightly from the curve fit, are subsets of the data recorded during a single acquisition period. Because this data acquisition period was not recorded after any severe flutter points and was recorded between other data sets that follow the general trend, they do not indicate a change in the dynamic properties of the model and PAPA system.

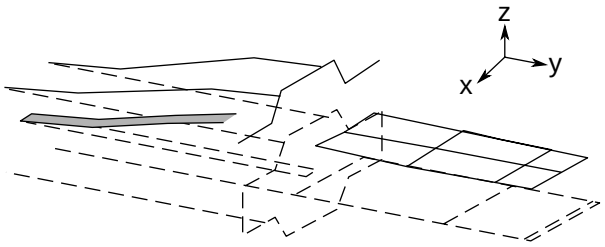

(a) Rigid-body plunge; frequency, 3.33 Hz.

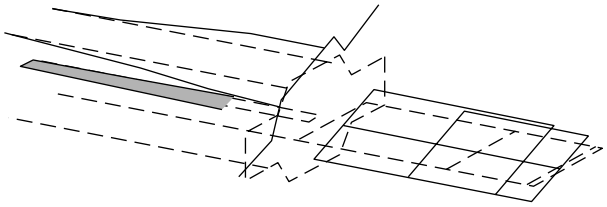

(b) Rigid-body pitch; frequency, 5.20 Hz.

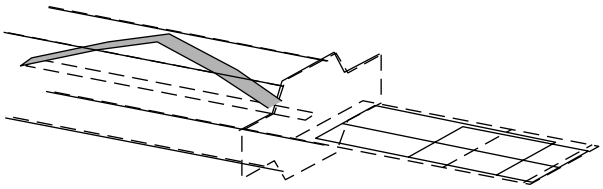

(c) First bending of drag strut; frequency, 37 Hz.

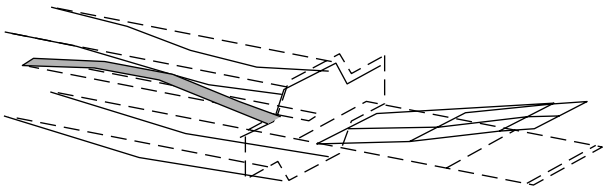

(d) Second bending of system; frequency, 50 Hz.

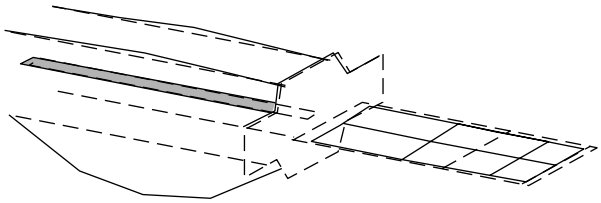

(e) Bending of rod 3; frequency, 75 Hz.

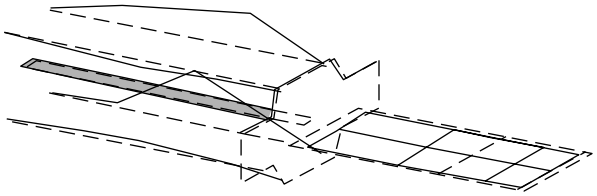

(f) Bending of rod 1 or 4; frequency, 78 Hz.

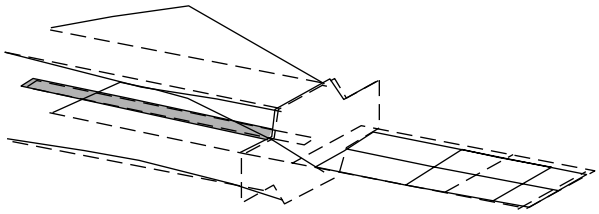

(g) Bending of rod 1 or 4; frequency, 79 Hz.

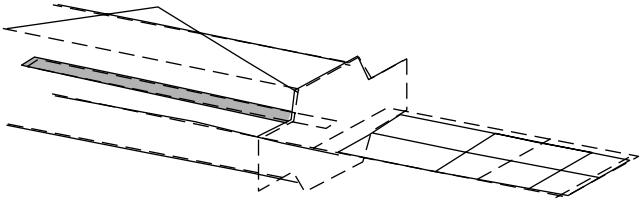

(h) Bending of rod 2; frequency, 81 Hz.

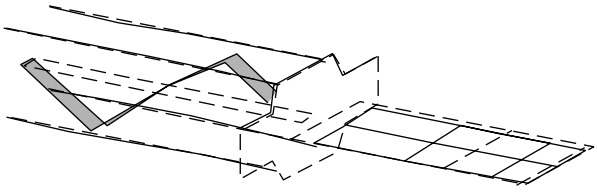

(i) Secondary bending of drag strut; frequency, 100 Hz.

Figure 16. Measured mode shapes.

Table 3. Bending and Torsion SGB Calibration Data

Leading-edge displacement, in.	Trailing-edge displacement, in.	Plunge loading, lb	Pitch moment, in-lb
First calibration			
0	0	0	0
.13	.007	20	200
.177	.179	40	0
.188	.266	50	−100
.269	.269	60	0
.356	.276	70	100
.366	.364	80	0
.443	.366	90	100
.45	.453	100	0
.382	.454	90	−100
.38	.379	80	0
.279	.364	70	−100
.278	.278	60	0
.195	.276	50	−100
.19	.189	40	0
.011	.178	20	−200
−.001	.001	0	0
Second calibration			
0	0	0	0
.173	.007	20	200
.17	−.162	0	400
.251	−.16	10	500
.251	−.247	0	600
.168	−.251	−10	500
.17	−.167	0	400
−.005	−.177	−20	200
−.001	−.002	0	0
−.17	−.005	−20	−200
−.161	.17	0	−400
−.231	.17	−10	−500
−.238	.251	0	−600
−.156	.251	10	−500
−.16	.175	0	−400
.009	.176	20	−200
−.001	−.001	0	0

Leading-edge displacement, in.	Trailing-edge displacement, in.	Plunge loading, lb	Pitch moment, in-lb
Third calibration			
0	0	0	0
.173	.007	20	200
.183	.182	40	0
.351	.19	60	200
.527	.198	80	400
.538	.374	100	200
.711	.384	120	400
.886	.494	140	600
.895	.568	160	400
.919	.92	200	0
.927	.774	180	200
.769	.768	160	0
.746	.576	140	200
.578	.573	120	0
.47	.475	100	0
.469	.39	90	100
.459	.287	80	200
.38	.287	70	100
.279	.28	60	0
.199	.28	50	−100
.106	.269	40	−200
.103	.19	30	−100
.095	.093	20	0
.009	.091	10	−100
.004	.003	0	0
Fourth calibration			
0	0	0	0
−.168	−.004	−20	−200
−.172	−.175	−40	0
−.331	−.174	−60	−200
−.481	−.17	−80	−400
−.459	−.321	−100	−200
−.387	−.428	−100	0
−.422	−.359	−90	−100
−.418	−.259	−80	−200
−.349	−.268	−70	−100
−.253	−.265	−60	0
−.181	−.265	−50	100
−.092	−.263	−40	200
−.091	−.178	−30	100
−.088	−.087	−20	0
−.005	−.087	−10	100
−.003	−.003	0	0
−.26	−.265	−60	0
−.001	−.002	0	0

Table 4. Plunge Mode Frequency and Damping Checks

Data set	f_z, Hz	ζ_z	A_z, in.
78A	3.335	1.06×10^{-3}	0.195
78B	3.335	1.05	.175
78C	3.335	1.02	.156
78D	3.336	1.00	.142
79A	3.339	.84	.050
79B	3.339	.84	.046
79C	3.339	.82	.042
79D	3.340	.82	.038
80A	3.341	.75	.017
80B	3.341	.74	.016
80C	3.341	.74	.015
80D	3.341	.74	.014
860A	3.326	1.71	.402
860B	3.326	1.35	.339
860C	3.327	1.32	.294
860D	3.327	1.28	.256
861A	3.329	1.02	.135
861B	3.330	.95	.121
861C	3.330	.90	.110
861D	3.330	.87	.100
862A	3.331	.80	.071
862B	3.332	.75	.065
862C	3.332	.77	.060
862D	3.332	.75	.055
282A	3.330	1.38	.353
282B	3.330	1.37	.305
282C	3.331	1.35	.265
282D	3.332	1.32	.233
283A	3.334	.96	.112
283B	3.335	.93	.101
283C	3.335	.91	.092
283D	3.335	.89	.084

Data set	f_z, Hz	ζ_z	A_z, in.
284A	3.337	0.81×10^{-3}	0.052
284B	3.337	.81	.048
284C	3.337	.79	.044
284D	3.337	.79	.041
346A	3.331	1.35	.353
346B	3.331	1.32	.306
346C	3.332	1.30	.267
346D	3.332	1.27	.236
347A	3.334	1.04	.144
347B	3.334	1.00	.129
347C	3.335	.97	.116
347D	3.335	.95	.106
348A	3.337	.86	.062
348B	3.337	.86	.057
348C	3.337	.83	.052
348D	3.337	.83	.048
781A	3.338	2.92	.023
781B	3.345	1.21	.017
781C	3.342	2.64	.015
781D	3.338	.38	.011
782A	3.335	.81	.088
782B	3.335	.79	.081
782C	3.335	.79	.074
782D	3.335	.79	.069
783A	3.337	.77	.044
783B	3.337	.75	.041
783C	3.337	.75	.038
783D	3.337	.74	.035

Table 5. Pitch Mode Frequency and Damping Checks

Data set	f_θ, Hz	ζ_θ	A_θ, in.
81A	5.202	0.64×10^{-3}	0.899
81B	5.202	.62	.827
81C	5.202	.60	.762
81D	5.202	.59	.705
81E	5.202	.57	.653
82A	5.202	.44	.340
82B	5.202	.43	.321
82C	5.202	.43	.304
82D	5.202	.42	.287
82E	5.202	.41	.272
83A	5.203	.38	.211
83B	5.203	.38	.201
83C	5.203	.37	.191
83D	5.203	.36	.182
83E	5.203	.35	.173
88A	5.249	1.73	3.926
88B	5.230	1.37	3.138
88C	5.219	1.18	2.622
88D	5.212	1.03	2.247
88E	5.207	.94	1.967
89A	5.200	.78	1.299
89B	5.199	.75	1.173
89C	5.198	.72	1.064
89D	5.198	.70	.968
89E	5.197	.67	.884
90A	5.197	.59	.490
90B	5.197	.59	.454
90C	5.197	.58	.421
90D	5.197	.57	.390
90E	5.197	.57	.362
85A	5.200	.82	1.446
85B	5.198	.79	1.300
85C	5.197	.76	1.173
85D	5.197	.73	1.062
85E	5.196	.71	.966
86A	5.195	.60	.535
86B	5.195	.59	.495
86C	5.196	.58	.458
86D	5.196	.58	.425
86E	5.196	.57	.394

Data set	f_θ, Hz	ζ_θ	A_θ, in.
87A	5.197	0.58×10^{-3}	0.231
87B	5.197	.58	.214
87C	5.197	.60	.198
87D	5.197	.61	.184
87E	5.197	.61	.170
49A	5.207	1.21	2.357
49B	5.202	1.09	2.013
49C	5.198	.97	1.747
49D	5.196	.91	1.539
49E	5.194	.86	1.367
50A	5.191	.67	.627
50B	5.191	.66	.575
50C	5.191	.65	.528
50D	5.191	.63	.485
50E	5.191	.63	.456
51A	5.192	.61	.245
51B	5.192	.62	.227
51C	5.192	.62	.209
51D	5.192	.62	.193
51E	5.193	.65	.178
84A	5.198	2.22	2.319
84B	5.193	1.74	1.749
84C	5.192	1.38	1.391
84D	5.192	1.02	1.170
84E	5.191	.95	1.024
185A	5.191	.71	.565
185B	5.191	.70	.515
185C	5.191	.68	.470
185D	5.192	.67	.430
185E	5.192	.67	.394
186A	5.193	.61	.240
186B	5.193	.60	.222
186C	5.194	.57	.205
186D	5.194	.53	.191
186E	5.194	.50	.178

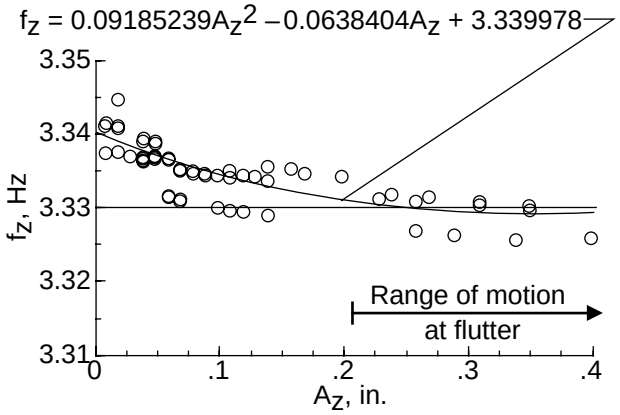

Figure 17. Wind-off frequency for plunge mode.

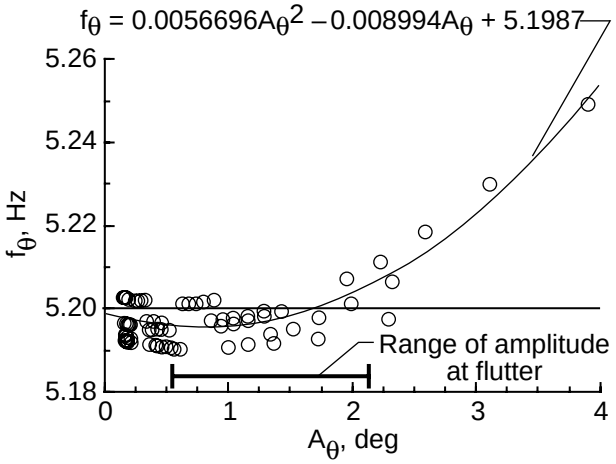

Figure 18. Wind-off frequency for pitch mode.

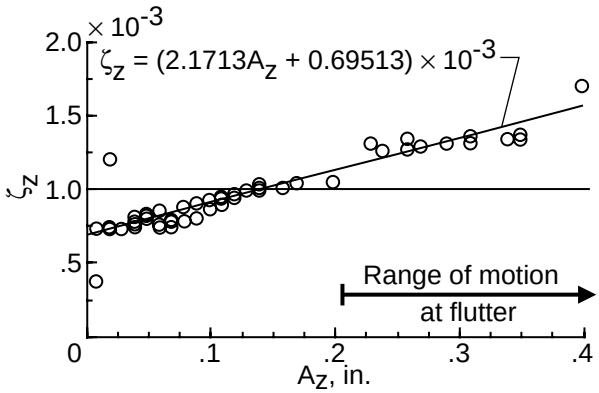

Figure 19. Wind-off damping for plunge mode.

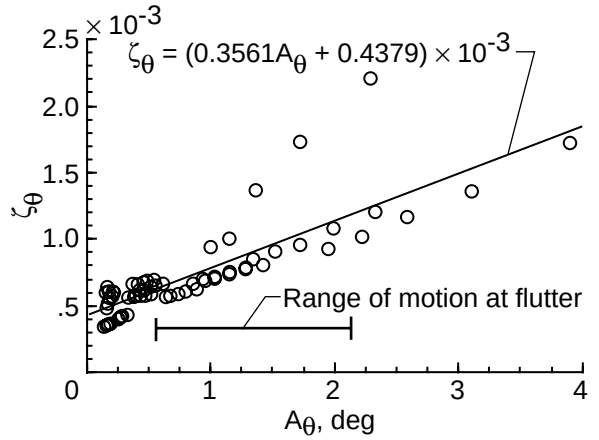

Figure 20. Wind-off damping for pitch mode.

Concluding Remarks

The Structural Dynamics Division of the Langley Research Center is conducting the Benchmark Models Program to acquire test data for the development and evaluation of aeroelastic computational fluid dynamics codes. The supercritical wing examined herein is the second in a series of three similar models that will provide simultaneous flutter and pressure data for use in code evaluation.

The supercritical wing, a rigid semispan model with a rectangular planform and a supercritical airfoil, was instrumented to measure surface pressures on both the upper surface and the lower surface at two spanwise stations. Planform data and surface measurements have been presented. Instrumentation for the measurement of model motion and model temperature was also discussed.

The rigid supercritical wing was flutter tested in the Langley Transonic Dynamics Tunnel using a flexible mount called the Pitch and Plunge Apparatus. This flexible mount, which provides a well-defined, two-degree-of-freedom dynamic system, was described and the experimentally determined dynamic characteristics of the model and mount system were presented. The results presented included frequency, stiffness, and structural damping for the rigid-body plunge and pitch modes as well as calculated values of generalized mass. Frequencies for all natural modes below 190 Hz and mode shapes for out-of-plane modes below 100 Hz were also presented.

NASA Langley Research Center
Hampton, VA 23681-0001
June 17, 1993

Appendix

Surface Measurements of Supercritical Wing Model

Included herein are the design airfoil coordinates, all the model surface measurements, and the measured locations of all the pressures orifices. In this appendix, the coordinate system for the tables originates at the intersection of the model leading edge and root chord. The x-axis is oriented for increasing positive values from model leading edge to model trailing edge. The y-axis is positive going from model root to model tip. For model surface measurements, positive z-axis values indicate upper-surface measurements while negative z-axis values correspond to lower-surface measurements.

The design airfoil coordinates are presented in table A1. These coordinates are based on coordinates given in reference 7. The measured locations of the 80 pressure orifices are presented in table A2. Table A3 gives the locations of the pressure orifices on the splitter plate, including those on the boundary-layer rake. Since the model and PAPA assembly moves relative to the splitter plate when a load is applied, the values given in this table assume a zero plunge loading condition.

The surface measurements are presented in tables A4 to A14. These measurements were made prior to wind-on flutter testing and are accurate to ± 0.0005 in. In the chordwise direction, measurements were made at eight spanwise stations. These measurements, which are presented in tables A4 to A11, document the airfoil shape at span stations near the model root chord ($y = 0.02$ and 1.6 in.), on either side of the two section breaks (which are located at $y = 20.6$ and 31.8 in.), and at the pressure measurement span stations ($y = 19.2$ and 30.4 in.). In these tables the deviation of the measured surface coordinate from the design airfoil shape in the z-direction is presented as Dev. Data points that deviate by more than 0.005 in. from the design are denoted by an asterisk.

Measurements of the surface shape of the tip cap, taken along 19 chordwise stations, can be found in table A12. Tables A13 and A14 present surface measurements obtained in the spanwise direction at two chordwise stations ($x = 0.8$ and 15.9 in.). The data in these tables extend from the wing root to the wing tip and cover both the upper surface and the lower surface.

Table A1. Design SC(2)-0414 Airfoil Coordinates

[Based on ref. 7]

x, in.	Upper-surface z, in.	Lower-surface z, in.
0.00	0.0000	0.0000
.03	.1728	−.1728
.08	.2656	−.2656
.16	.3600	−.3600
.32	.4784	−.4784
.48	.5600	−.5600
.80	.6736	−.6736
1.12	.7536	−.7552
1.44	.8160	−.8192
1.76	.8672	−.8720
2.08	.9104	−.9168
2.40	.9472	−.9552
2.72	.9792	−.9888
3.04	1.0064	−1.0176
3.52	1.0416	−1.0528
4.00	1.0688	−1.0800
4.48	1.0896	−1.1008
4.96	1.1056	−1.1136
5.44	1.1152	−1.1200
5.60	1.1184	−1.1200
5.92	1.1216	−1.1184
6.40	1.1232	−1.1120
6.56	1.1232	−1.1088
6.88	1.1200	−1.0976
7.20	1.1152	−1.0832
7.52	1.1088	−1.0656
7.84	1.0992	−1.0416
8.00	1.0944	−1.0272
8.16	1.0880	−1.0128
8.48	1.0752	−.9792
8.80	1.0592	−.9392
9.12	1.0400	−.8928
9.44	1.0176	−.8432
9.76	.9920	−.7872
10.08	.9632	−.7280
10.40	.9328	−.6640
10.72	.8992	−.5968
11.04	.8640	−.5280
11.36	.8256	−.4576
11.68	.7840	−.3872
12.00	.7424	−.3168
12.32	.6976	−.2496
12.64	.6512	−.1856
12.96	.6032	−.1248
13.28	.5536	−.0688
13.60	.5024	−.0192
13.92	.4496	.0208
14.24	.3952	.0512
14.56	.3376	.0704
14.88	.2800	.0736
15.20	.2192	.0608
15.52	.1552	.0336
15.84	.0880	−.0128
16.00	.0528	−.0432

Table A2. Measured Distribution of Surface Pressure Orifices

x/c at $y = 19.2$ in.		x/c at $y = 30.4$ in.	
Upper surface	Lower surface	Upper surface	Lower surface
0.000		0.000	
.009	0.012	.009	0.012
.023	.027	.024	.027
.049	.053	.049	.052
.099	.103	.098	.102
.149		.148	
.198	.203	.198	.203
.249		.248	
.298	.303	.298	.303
.348		.348	
.398	.403	.398	.403
.448		.448	
.498	.503	.498	.503
.542	.552	.542	.552
.598	.602	.598	.602
.648	.652	.648	.652
.698	.702	.698	.702
.749	.752	.748	.751
.799	.801	.798	.800
.849	.851	.848	.850
.899	.901	.898	.900
.950	.941	.950	.940
1.000		1.000	

Table A3. Locations of Pressure Measurements on Splitter Plate

x, in.	y, in.	z, in.
Horizontal row		
48	0	0
32	0	0
8	0	0
4	0	0
0	0	0
−16	0	0
−20	0	0
−24	0	0
−48	0	0
−64	0	0
Vertical row 1		
0	0	16
0	0	8
0	0	4
0	0	−4
0	0	−16
Vertical row 2		
−16	0	16
−16	0	8
−16	0	4
−16	0	−4
−16	0	−16
Rake		
−32	0.25	16
−32	.50	16
−32	.75	16
−32	1.00	16
−32	1.50	16
−32	2.00	16
−32	2.50	16
−32	3.00	16
−32	4.00	16
−32	5.00	16

References

1. Edwards, John W.; and Malone, John B.: Current Status of Computational Methods for Transonic Unsteady Aerodynamics and Aeroelastic Applications. *Transonic Unsteady Aerodynamics and Aeroelasticity*, AGARD-CP-507, Mar. 1992, pp. 1-2–1-20.

2. Bennett, Robert M.; Eckstrom, Clinton V.; Rivera, José A., Jr.; Dansberry, Bryan E.; Farmer, Moses G.; and Durham, Michael H.: *The Benchmark Aeroelastic Models Program: Description and Highlights of Initial Results.* NASA TM-104180, 1991.

3. Durham, Michael H.; Keller, Donald F.; Bennett, Robert M.; and Wieseman, Carol D.: A Status Report on a Model for Benchmark Active Controls Testing. AIAA-91-1011, Apr. 1991.

4. Rivera, José A., Jr.; Dansberry, Bryan E.; Bennett, Robert M.; Durham, Michael H.; and Silva, Walter A.: *NACA0012 Benchmark Model Experimental Flutter Results With Unsteady Pressure Distributions.* NASA TM-107581, 1992. (Also available as AIAA-92-2396.)

5. Rivera, José A., Jr.; Dansberry, Bryan E.; Durham, Michael H.; Bennett, Robert M.; and Silva, Walter A.: *Pressure Measurements on a Rectangular Wing With a NACA0012 Airfoil During Conventional Flutter.* NASA TM-104211, 1992.

6. Bennett, Robert M.; Dansberry, Bryan E.; Farmer, Moses G.; Eckstrom, Clinton V.; Seidel, David A.; and Rivera, José A., Jr.: *Transonic Shock-Induced Dynamics of a Flexible Wing With a Thick Circular-Arc Airfoil.* NASA TM-104088, 1991. (Also available as AIAA-91-1107.)

7. Harris, Charles D.: *NASA Supercritical Airfoils—A Matrix of Family-Related Airfoils.* NASA TP-2969, 1990.

8. Farmer, Moses G.: *A Two-Degree-of-Freedom Flutter Mount System With Low Damping for Testing Rigid Wings at Different Angles of Attack.* NASA TM-83302, 1982.

9. Farmer, Moses G.: Model Mount System for Testing Flutter. U.S. Patent No. 4,475,385, Oct. 9, 1984.

Table A4. Chordwise Airfoil Measurements at $y = 0.02$ in.

Table A4. Continued

Table A4. Continued

Table A4. Concluded

Table A5. Chordwise Airfoil Measurements at $y = 1.6$ in.

Table A5. Continued

Table A5. Continued

Table A5. Concluded

Table A6. Chordwise Airfoil Measurements at $y = 19.2$ in.

Table A6. Continued

Table A6. Continued

Table A6. Concluded

Table A7. Chordwise Airfoil Measurements at $y = 20.58$ in.

Table A7. Continued

Table A7. Continued

Table A7. Concluded

Table A8. Chordwise Airfoil Measurements at $y = 20.62$ in.

Table A8. Continued

Table A8. Continued

Table A8. Concluded

Table A9. Chordwise Airfoil Measurements at $y = 30.4$ in.

Table A9. Continued

Table A9. Continued

Table A9. Concluded

Table A10. Chordwise Airfoil Measurements at $y = 31.78$ in.

Table A10. Continued

Table A10. Continued

Table A10. Concluded

Table A11. Chordwise Airfoil Measurements at $y = 31.84$ in.

Table A11. Continued

Table A11. Continued

Table A11. Concluded

Table A12. Tip of Revolution Measurements

Table A13. Spanwise Airfoil Measurements at $x = 0.8$ in.

Table A13. Continued

Table A13. Continued

Table A13. Continued

Table A13. Continued

Table A13. Continued

Table A13. Continued

Table A13. Concluded

Table A14. Spanwise Airfoil Measurements at $x = 15.9$ in.

Table A14. Concluded

REPORT DOCUMENTATION PAGE

Form Approved
OMB No. 0704-0188

1. AGENCY USE ONLY *(Leave blank)*	2. REPORT DATE	3. REPORT TYPE AND DATES COVERED
	September 1993	Technical Memorandum

4. TITLE AND SUBTITLE
Physical Properties of the Benchmark Models Program Supercritical Wing

5. FUNDING NUMBERS
WU 505-63-50-16

6. AUTHOR(S)
Bryan E. Dansberry, Michael H. Durham, Robert M. Bennett, David L. Turnock, Walter A. Silva, and José A. Rivera, Jr.

7. PERFORMING ORGANIZATION NAME(S) AND ADDRESS(ES)
NASA Langley Research Center
Hampton, VA 23681-0001

8. PERFORMING ORGANIZATION REPORT NUMBER
L-17177

9. SPONSORING/MONITORING AGENCY NAME(S) AND ADDRESS(ES)
National Aeronautics and Space Administration
Washington, DC 20546-0001

10. SPONSORING/MONITORING AGENCY REPORT NUMBER
NASA TM-4457

11. SUPPLEMENTARY NOTES
Dansberry, Durham, Bennett, Silva, and Rivera: Langley Research Center, Hampton, VA; Turnock: Lockheed Engineering & Sciences Co., Hampton, VA.

12a. DISTRIBUTION/AVAILABILITY STATEMENT
Unclassified–Unlimited

Subject Category 05

12b. DISTRIBUTION CODE

13. ABSTRACT *(Maximum 200 words)*
The goal of the Benchmark Models Program is to provide data useful in the development and evaluation of aeroelastic computational fluid dynamics (CFD) codes. To that end, a series of three similar wing models are being flutter tested in the Langley Transonic Dynamics Tunnel. These models are designed to simultaneously acquire model response data and unsteady surface pressure data during wing flutter conditions. The supercritical wing is the second model of this series. It is a rigid semispan model with a rectangular planform and a NASA SC(2)-0414 supercritical airfoil shape. The supercritical wing model was flutter tested on a flexible mount, called the Pitch and Plunge Apparatus, that provides a well-defined, two-degree-of-freedom dynamic system. This report describes the supercritical wing model and associated flutter test apparatus and includes experimentally determined wind-off structural dynamic characteristics of the combined rigid model and flexible mount system.

14. SUBJECT TERMS
Aeroelasticity; Experimental data; Structural dynamics; Transonic; Benchmark Models Program

15. NUMBER OF PAGES
61

16. PRICE CODE
A04

17. SECURITY CLASSIFICATION OF REPORT	18. SECURITY CLASSIFICATION OF THIS PAGE	19. SECURITY CLASSIFICATION OF ABSTRACT	20. LIMITATION OF ABSTRACT
Unclassified	Unclassified		